nature immunology

Rapid effector function of memory CD8+ T cells requires an immediate-early glycolytic switch

Patrick M Gubser[1,2], Glenn R Bantug[1,2], Leyla Razik[1], Marco Fischer[1], Sarah Dimeloe[1], Gideon Hoenger[1], Bojana Durovic[1], Annaïse Jauch[1] & Christoph Hess[1]

Antigen-experienced memory T cells acquire effector function with innate-like kinetics; however, the metabolic requirements of these cells are unknown. Here we show that rapid interferon-γ (IFN-γ) production of effector memory (EM) CD8+ T cells, activated through stimulation mediated by the T cell antigen receptor (TCR) and the costimulatory receptor CD28 or through cognate interactions, was linked to increased glycolytic flux. EM CD8+ T cells exhibited more glyceraldehyde-3-phosphate dehydrogenase (GAPDH) activity at early time points, before proliferation commenced, than did naive cells activated under similar conditions. CD28 signaling via the serine-threonine kinase Akt and the metabolic-checkpoint kinase mTORC2 was needed to sustain TCR-mediated immediate-early glycolysis. Unlike glycolysis in proliferating cells, immediate-early glycolysis in memory CD8+ T cells was rapamycin insensitive. Thus, CD8+ memory T cells have an Akt-dependent 'imprinted' glycolytic potential that is required for efficient immediate-early IFN-γ recall responses.

During acute viral infection, pathogen-specific naive CD8+ T cells become activated, followed by clonal expansion and differentiation into cytotoxic effector cells[1]. Resolution of infection triggers the contraction of effector cell populations, accompanied by the formation of a long-lived memory pool[2]. In a highly coordinated process, memory CD8+ T cells subsequently enhance host protection after secondary infection (recall response)[2].

Naive and memory CD8+ T cells are metabolically quiescent cells, which depend mainly on oxidative phosphorylation as their energy source[3–5]. Ligation of the T cell antigen receptor (TCR) and subsequent costimulation of quiescent cells initiates substantial changes in cellular metabolic pathway use[6,7]. Upregulation of aerobic glycolysis (the Warburg effect) is an important feature of this metabolic adaptation and is a prerequisite for the growth and population expansion of CD8+ T cells[7–9]. Augmented glycolysis by proliferating cells is linked to enhanced glucose uptake and increased expression and activity of glycolytic enzymes, whereas glucose use via oxidative phosphorylation is decreased[10,11]. This 'metabolic switch' satiates higher energy demands and provides biochemical intermediates used in the biosynthesis of macromolecules[12].

The early recall phase of an immune response relies on antigen-experienced T cells that are able to acquire effector function with 'innate-like' response kinetics[13]. Effector memory (EM) CD8+ T cells are specialized antigen-experienced lymphocytes that traffic between blood and nonlymphoid tissues[14–17]. EM CD8+ T cells are ideally positioned to rapidly respond and execute effector functions at sites of infection. The metabolic requirements that support this pivotal immediate-early memory functionality are not known.

In this report, we postulate that the 'innate-like' response kinetics of EM CD8+ T cells is coupled to 'imprinted' metabolic features that enable the very rapid acquisition of effector functionality. We characterize differences between naive and EM human CD8+ T cells in their use of the glycolytic pathway after drug-induced mitochondrial stress and immediately after stimulation mediated by the TCR and coreceptor CD28. Finally, we assess how glycolysis during this immediate-early activation phase is regulated and linked to recall responses of CD8+ T cells.

RESULTS

Metabolic profiles of naive and EM CD8+ T cells

We sorted freshly isolated cells into CD45RA+CCR7+ (naive) and CD45RA−CCR7− (EM) populations[14] (**Supplementary Fig. 1**). We used metabolic-flux analysis (with the Seahorse XF Analyzer) to assess mitochondrial respiration and aerobic glycolysis by measuring the oxygen-consumption rate (OCR) and extracellular acidification rate (ECAR), respectively, under basal conditions and after drug-induced mitochondrial stress[18] (**Supplementary Fig. 2**). Basal respiration was similar in naive and EM populations (**Fig. 1a**,**b**). Moreover, there was no measurable difference between naive and EM CD8+ T cells in their ATP-coupled, leak and non-mitochondrial respiration (**Supplementary Fig. 3**). We detected a small but significant increase in spare respiratory capacity in EM CD8+ T cells relative to that in naive CD8+ T cells (**Fig. 1a**,**c**). In agreement with that finding, increased spare respiratory capacity has been described as a key component of memory formation in mouse CD8+ T cells[19].

Basal glycolysis, as demonstrated by ECAR, was similar and low in naive and EM CD8+ T cells (**Fig. 1d**,**e**). However, after pharmacological

[1]Department of Biomedicine, Immunobiology, University of Basel, Basel, Switzerland. [2]These authors contributed equally to this work. Correspondence should be addressed to C.H. (chess@uhbs.ch).

Received 26 February; accepted 12 July; published online 18 August 2013; doi:10.1038/ni.2687

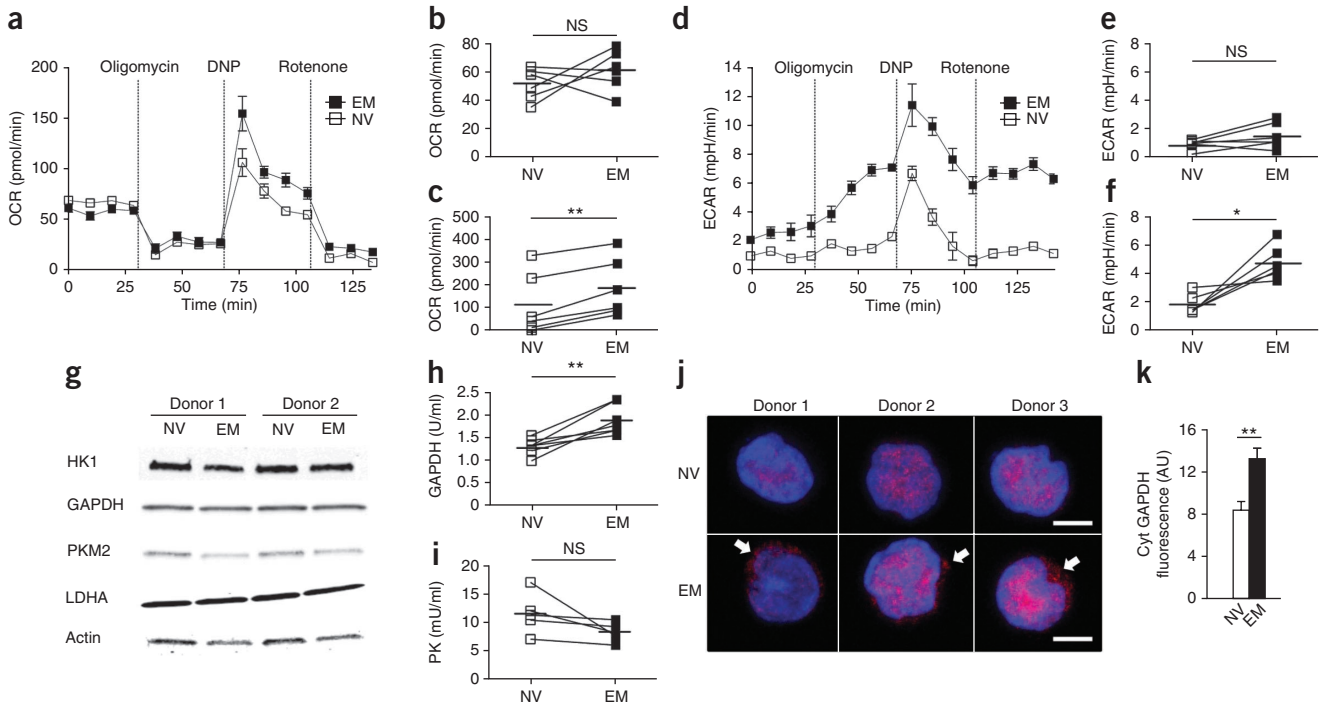

Figure 1 Naive and EM CD8$^+$ T cells display distinct oxidative and glycolytic capacities. (**a**) OCR of naive (NV) and EM CD8$^+$ T cells (from one of six donors) in real time after the addition of oligomycin, 2,4–dinitrophenol (DNP) and rotenone. (**b**,**c**) Mean basal (**b**) and spare (**c**) respiratory capacity of the cells in **a** ($n = 6$ donors). (**d**) ECAR of naive and EM CD8$^+$ T cells (from one of six donors) in real time after treatment as in **a**. (**e**,**f**) Mean basal (**e**) and maximal (**f**) ECAR of the cells in **d** ($n = 6$ donors). (**g**) Immunoblot analysis of glycolytic enzymes in lysates of naive and EM CD8$^+$ T cells (two of three donors; top); actin serves as a loading control. (**h**,**i**) Activity of GAPDH (**h**; $n = 7$ donors) and PK (**i**; $n = 5$ donors) in lysates of naive and EM CD8$^+$ T cells. (**j**) Stacked confocal microscopy of naive and EM CD8$^+$ T cells ($n = 3$ donors) stained with anti-GAPDH (red) and counterstained with the DNA-intercalating dye DAPI (blue; nucleus). Arrows indicate GAPDH in the cytoplasm. Original magnification, ×100. Scale bars, 3 μm. (**k**) Fluorescence intensity of cytoplasmic (Cyt) GAPDH in naive CD8$^+$ T cells ($n = 36$) and EM CD8$^+$ T cells ($n = 53$) from three donors, presented in arbitrary units (AU). Each symbol (**b**,**c**,**e**,**f**,**h**,**i**) represents an individual donor; small horizontal lines indicate the mean. NS, not significant; $^*P < 0.01$ and $^{**}P < 0.001$ (paired two-tailed Student's *t*-test (**b**,**c**,**e**,**f**,**h**,**i**) or Mann-Whitney *U*-test (**k**)). Data are representative of six (**a**–**f**), three (**g**,**j**,**k**), seven (**h**) or five (**i**) experiments (all one experiment per donor; mean and s.e.m. in **a**,**d**,**k**).

inhibition of mitochondrial respiration, the ECAR of EM CD8$^+$ T cells rapidly increased, whereas naive CD8$^+$ T cells maintained their glycolytic rate (**Fig. 1d**,**f**). There was no difference between the subsets in cell viability after inhibition of mitochondrial respiration (data not shown).

Total cellular protein expression of several enzymes along the glycolytic pathway (hexokinase 1 (HK1), glyceraldehyde-3-phosphate dehydrogenase (GAPDH), pyruvate kinase isoform M2 (PKM2) and lactate dehydrogenase A (LDHA)) was similar in naive and EM CD8$^+$ T cells (**Fig. 1g**). This indicated that the glycolytic machinery was present in both CD8$^+$ T cell subsets. However, the kinetics with which EM CD8$^+$ T cells were able to increase glycolysis suggested 'imprinted' metabolic features immediately able to support increased glycolytic activity. Therefore, we assessed the activity of GAPDH, a key glycolytic enzyme that initiates the ATP-generation phase of the pathway, and pyruvate kinase (PK), an enzyme that catalyzes a major rate-limiting step in the glycolytic pathway, in freshly sorted naive and EM CD8$^+$ T cells. Basal GAPDH activity was consistently higher in EM CD8$^+$ T cells (**Fig. 1h**), whereas we detected no significant difference between the subsets in their PK enzymatic activity (**Fig. 1i**). In addition to its well-established metabolic role, GAPDH also has nuclear functions[20]. Moreover, several studies have demonstrated that cytoplasmic GAPDH possesses higher glycolytic activity than does nuclear GAPDH[21]. Given the incongruent findings on the protein abundance and activity of GAPDH, we therefore assessed the intracellular distribution of GAPDH. GAPDH was localized mainly in the nucleus of naive CD8$^+$ T cells but was present both in the nucleus and the cytoplasm of EM CD8$^+$ T cells (**Fig. 1j**,**k**). Collectively, these findings identified enhanced glycolytic capacity in EM CD8$^+$ T cells, as demonstrated by higher cytoplasmic localization and activity of GAPDH, which was rapidly used under conditions of mitochondrial stress.

Activation-induced immediate-early glycolytic switch

We next used an 'in-Seahorse' activation system to investigate how readily aerobic glycolysis is accessed by quiescent naive and EM CD8$^+$ T cells after stimulation via the TCR and CD28. In this assay, we applied monoclonal antibody (mAb) to CD3 (anti-CD3) and mAb to CD28 (anti-CD28) directly onto plated cells and monitored the ECAR in real time. After injection of both antibodies, we observed a rapid rise in the ECAR of naive and EM CD8$^+$ T cells (**Fig. 2a**). The ECAR increase in naive cells was transient and rapidly returned to baseline (**Fig. 2a**,**b**). In contrast, the enhanced ECAR of EM CD8$^+$ T cells remained stable over the duration of the assay (**Fig. 2a**,**c**). Contrary to published studies[6,7,22], these experiments were able to identify the unique ability of activated EM CD8$^+$ T cells to rapidly activate and sustain aerobic glycolysis (the 'immediate-early glycolytic switch'). CD28 had high expression on naive and EM CD8$^+$ T cells, albeit slightly more on EM cells than on naive cells (**Supplementary Fig. 4a–c**). The EM cell–specific ability to sustain the ECAR could

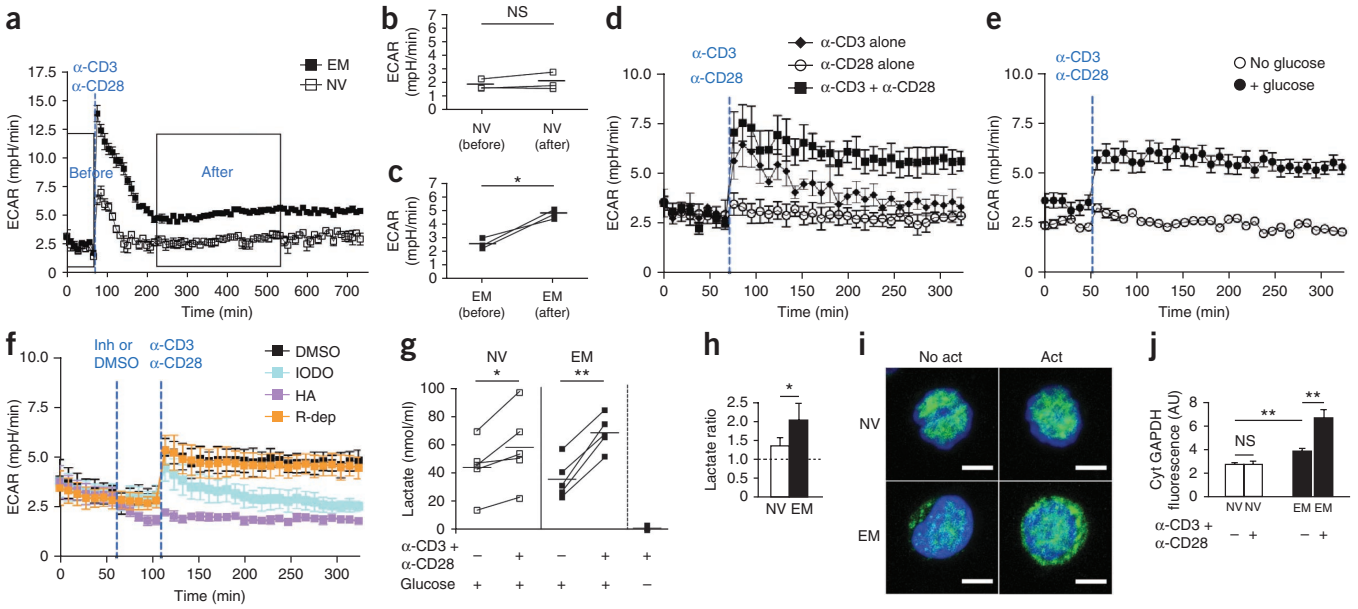

Figure 2 The activation-induced immediate-early glycolytic switch is intrinsic to EM CD8$^+$ T cells. (**a**) ECAR of naive and EM CD8$^+$ T cells (from one of three donors) before and after 'in-Seahorse' activation with anti-CD3 (α-CD3; 0.2 μg/ml) and anti-CD28 (α-CD28; 20 μg/ml); boxes outline ECAR values used for calculation of means before and after injection. (**b**,**c**) Mean ECAR values before and after injection of anti-CD3 plus anti-CD28 onto plated naive CD8$^+$ T cells (**b**) or EM CD8$^+$ T cells (**c**) ($n = 3$ donors); titration experiments with up to 2 μg/ml of anti-CD3 and down to 10 μg/ml of anti-CD28 yielded similar results (not shown). (**d**) ECAR of EM CD8$^+$ T cells activated with anti-CD3 (2 μg/ml) or anti-CD28 (20 μg/ml) alone or the mAbs together (key). (**e**) ECAR of bulk CD8$^+$ T cells activated with anti-CD3 (1 μg/ml) and anti-CD28 (10 μg/ml) in the presence of 10 mM glucose (+ glucose) or glucose-free medium (No glucose). (**f**) ECAR of bulk CD8$^+$ T cells pretreated with dimethyl sulfoxide (DMSO) or the inhibitor (Inh) iodoacetate (IODO; 10 μM), heptelidic acid (HA; 10 μM) or *R*-(−)-deprenyl hydrochloride (R-dep; 10 nM) before activation as in **e**. (**g**) Quantification of lactate in the medium of naive and EM CD8$^+$ T cells ($n = 5$ donors) left nonactivated (−) or activated (+) with anti-CD3 (2 μg/ml) plus anti-CD28 (20 μg/ml) with or without glucose (bottom row). (**h**) Linear-regression analysis of the lactate concentrations in **g**, presented as lactate in activated cells/lactate in nonactivated cells. (**i**) Microscopy of naive and EM CD8$^+$ T cells left nonactivated (No act) or activated (Act) for 2 h with anti-CD3 (2 μg/ml) and anti-CD28 (20 μg/ml): green, GAPDH; blue, DAPI. Scale bars, 3 μm. (**j**) Fluorescence intensity of cytoplasmic GAPDH in naive and EM CD8$^+$ T cells left nonactivated (−) or stimulated (+) for 2 h with anti-CD3 (2 μg/ml) plus anti-CD28 (20 μg/ml); total cells: $n = 30$ (nonactivated naive), 43 (activated naive), 47 (nonactivated EM) or 70 (activated EM). Each symbol (**b**,**c**,**g**) represents an individual donor; small horizontal lines indicate the mean. $*P < 0.05$ and $**P < 0.001$ (paired two-tailed Student's *t*-test (**b**,**c**,**g**), linear-regression analysis (**h**) or Mann-Whitney *U*-test (**j**)). Data are representative of three experiments (**a**–**d**,**i**,**j**), one experiment (**e**), four experiments (**f**) or five experiments (**g**,**h**; all one experiment per donor; mean and s.e.m. in **a**,**d**–**f**,**h**,**j**).

potentially relate to differences in cell-surface expression of CD28. The activation of EM CD8$^+$ T cells solely with anti-CD3 triggered only a transient increase in the ECAR (**Fig. 2d**). Moreover, there was no detectable increase after treatment of EM CD8$^+$ T cells with anti-CD28 alone (**Fig. 2d**) or with anti-CD28 plus an isotype-matched control mAb in place of anti-CD3 (**Supplementary Fig. 5**). Thus, both TCR- and CD28-mediated signals were essential for the sustained immediate-early glycolytic switch in EM CD8$^+$ T cells. To verify that the increase in the ECAR was due to enhanced glucose metabolism, we did 'in-Seahorse' T cell–activation assays in glucose-free medium. The activation of bulk CD8$^+$ T cells in glucose-free medium completely abolished the expected increase in the ECAR (**Fig. 2e**). Pretreatment of bulk CD8$^+$ T cells with mechanistically distinct inhibitors of GAPDH (iodoacetate and heptelidic acid) diminished and blocked, respectively, the activation-induced glycolytic switch of CD8$^+$ T cells stimulated with anti-CD3 plus anti-CD28. Pretreatment of cells with *R*-(−)-deprenyl hydrochloride, which inhibits the translocation of GAPDH to the nucleus but not its enzymatic activity[23], did not affect the immediate-early glycolytic switch (**Fig. 2f**). We also observed inhibition of the immediate-early glycolytic switch in EM CD8$^+$ T cells treated with the hexokinase inhibitor 2-deoxy-D-glucose (2-DG; data not shown).

As an independent measure of aerobic glycolysis, we further assessed lactate production by nonactivated naive and EM CD8$^+$ T cells and those stimulated with anti-CD3 plus anti-CD28. In line with the ECAR data, lactate production by activated naive and EM CD8$^+$ T cells was greater than that of their nonactivated counterparts (**Fig. 2g**). Paired linear-regression analysis further established that the increase in lactate concentration was significantly greater in the supernatants of EM CD8$^+$ T cells than in those of naive CD8$^+$ T cells (**Fig. 2h**). The activation of EM CD8$^+$ T cells in glucose-free medium resulted in nearly undetectable lactate production (**Fig. 2g**). Together these experiments identified an immediate-early ability of EM CD8$^+$ T cells to take up and metabolize glucose in a sustained manner. Additionally, these results demonstrated that CD28 signaling was critical for sustaining the immediate-early glycolytic switch of EM CD8$^+$ T cells.

The sensitivity of immediate-early glycolysis to changes in GAPDH activity and the greater cytoplasmic localization of GAPDH in EM CD8$^+$ T cells suggested a critical role for this enzyme on maintenance of the immediate-early glycolytic switch in EM CD8$^+$ T cells. To assess cytoplasmic GAPDH expression under activating conditions, we incubated naive and EM CD8$^+$ T cells for 2 h with anti-CD3 plus anti-CD28 and assessed GAPDH localization by confocal microscopy. GAPDH remained confined to the nuclear compartment in activated naive CD8$^+$ T cells (**Fig. 2i**,**j**). In contrast, cytoplasmic expression of GAPDH was significantly enhanced in activated EM CD8$^+$ T cells (**Fig. 2i**,**j**). These findings indicated that the localization of GAPDH in the cytoplasm of EM CD8$^+$ T cells was regulated by stimulation via TCR-CD28. Moreover, maintenance of immediate-early

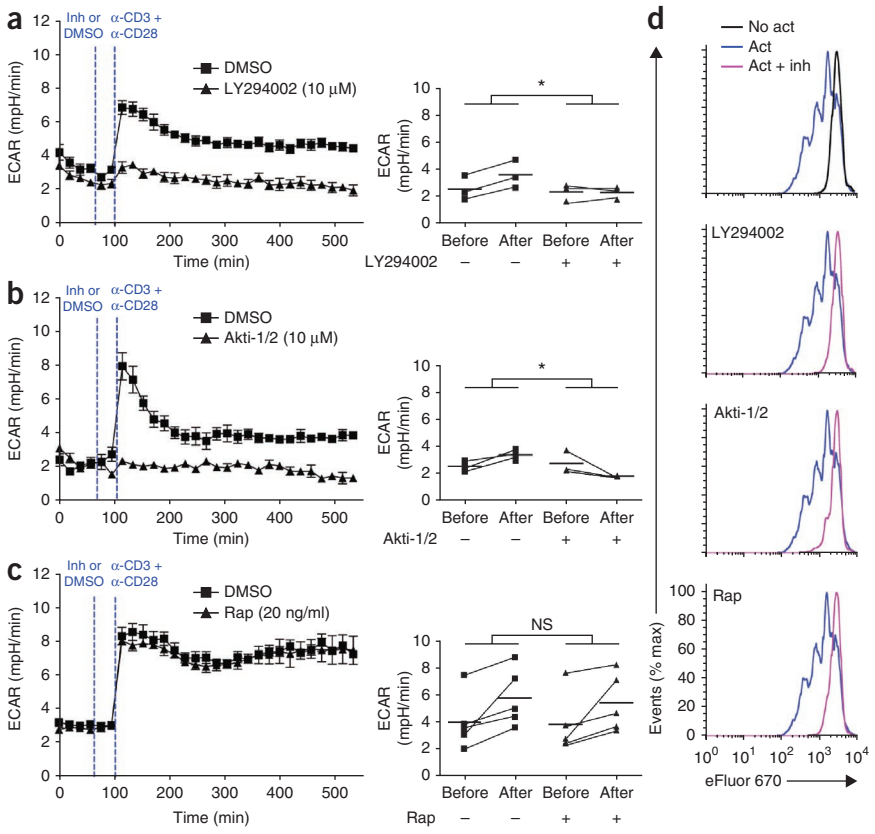

Figure 3 The immediate-early glycolytic switch in EM CD8$^+$ T cells is insensitive to inhibition of mTORC1 but is dependent on Akt activity. (**a**–**c**) ECAR (left); one of three to five donors and mean ECAR before and after activation (right; as in **Fig. 2**) of EM CD8$^+$ T cells pretreated with control medium (DMSO) or LY294002 (**a**), Akti-1/2 (**b**) or rapamycin (Rap) (**c**) before activation with anti-CD3 (1 μg/ml) and anti-CD28 (10 μg/ml); linear-regression analyses compare changes in mean ECAR between untreated and inhibitor-treated EM CD8$^+$ T cells. Each symbol represents an individual donor (n = 3–5); small horizontal lines indicate the mean. (**d**) Flow cytometry of EM CD8$^+$ T cells loaded with the cell-proliferation dye eFluor 670 and then left nonactivated (No act) or activated for 3 d with anti-CD3 plus anti-CD28 alone (Act) or in the presence of inhibitor (Act + inh). *P < 0.001 (linear-regression analysis). Data are representative of three to five experiments (**a**–**c**; mean and s.e.m.) or four experiments (**d**; all one experiment per donor).

glycolysis in EM CD8$^+$ T cells was potentially supported by increased localization of GAPDH in the cytoplasm.

Kinase Akt signaling and immediate-early glycolytic switch

Costimulation of CD28 during T cell activation enhances glucose use through signaling along the pathway that leads from phosphatidylinositol-3-OH kinase (PI(3)K) to the kinase Akt to the nutrient and energy sensor mTORC1, which leads to increased cell growth and proliferation[6,7,24]. The signaling events downstream of CD28 critical for the sustained immediate-early glycolytic switch in EM CD8$^+$ T cells are not known. To address this issue, we pretreated EM CD8$^+$ T cells with LY294002 (an inhibitor of PI(3)K), Akti-1/2 (an inhibitor of Akt), or rapamycin (an inhibitor of mTORC1), followed by 'in-Seahorse' activation experiments. Inhibition of PI(3)K (**Fig. 3a**) or Akt (**Fig. 3b**) abolished the activation-induced, immediate-early glycolytic switch in EM CD8$^+$ T cells. The diminution of the ECAR after inhibition of PI(3)K or Akt was not due to a decrease in cell viability, as the OCR remained stable for the duration of the assay (data not shown). Notably, the immediate-early glycolytic switch was refractory to rapamycin treatment (**Fig. 3c**). It is well established that LY294002 has an off-target inhibitory effect on mTORC1 (ref. 25). As rapamycin had no effect on the immediate-early glycolytic switch, we ruled out the possibility that this off-target effect was a confounder in these experiments. Because mTORC1 is a known regulator of glucose metabolism in proliferating T cells[11,26,27], we investigated the effect of rapamycin on the glycolytic capacity of naive and EM CD8$^+$ T cells after prolonged activation. The ECAR was enhanced in both naive and EM cells stimulated for 3 d with anti-CD3 plus anti-CD28 relative to the ECAR of unstimulated cells (**Supplementary Fig. 6**). However, after activation in the presence of rapamycin, the ECAR was much lower (**Supplementary Fig. 6**), which indicated that the protracted phase of aerobic glycolysis was sensitive to inhibition of mTORC1 in each subset of cells. Aerobic glycolysis is essential for providing energy and metabolic intermediates to highly proliferating cells[12]. In the presence of inhibitors of PI(3)K, Akt or mTORC1, the proliferation of EM CD8$^+$ T cells was blocked (**Fig. 3d**).

Finally, given the rapid increase in cytoplasmic GAPDH after the activation of EM CD8$^+$ T cells (**Fig. 2i,j**), we also assessed whether the cytoplasmic expression of GAPDH was dependent on Akt signaling. Pretreatment of EM CD8$^+$ T cells with Akti-1/2 resulted in much lower cytoplasmic expression of GAPDH mediated by anti-CD3 plus anti-CD28 (pooled results for cells from three donors; **Supplementary Fig. 7**). However, the effect of Akti-1/2 on cytoplasmic GAPDH expression was less robust than its effect on the glycolytic switch (**Fig. 3b**). Together these results indicated that the PI(3)K-Akt-mTORC1 pathway was essential for the population expansion of human EM CD8$^+$ T cells after stimulation via TCR and CD28, potentially through regulating aerobic glycolysis in highly proliferating CD8$^+$ T cells. Through the use of metabolic-flux analysis, we discriminated two distinct glycolytic phases in EM CD8$^+$ T cells: a rapamycin-insensitive immediate-early phase, and a rapamycin-sensitive protracted phase essential for the support of CD8$^+$ T cell proliferation.

The abrogation of glycolysis in EM CD8$^+$ T cells pretreated with LY294002 or Akti-1/2 indicated a central role for Akt in regulating the immediate-early glycolytic switch. Akt activity is dependent on the phosphorylation of two amino acid residues: Thr308 and Ser473. Akt Thr308 is a target of the phosphoinositide-dependent kinase PDK1, and Akt Ser473 is phosphorylated by mTORC2, which allows Akt to act on additional substrates involved in the metabolism and survival of cells[28]. Additionally, mTORC2 activity has been shown to be activated directly by the PI(3)K product phosphatidylinositol-(3,4,5)-trisphosphate[29]. Thus, PI(3)K could also affect Akt activation by modulating mTORC2 activity. To investigate the potential role of mTORC2 in the immediate-early glycolytic switch, we pretreated EM CD8$^+$ T cells with OSI-027, an mTORC1-mTORC2 inhibitor[30], and assayed changes in the ECAR after activation with anti-CD3 plus anti-CD28, as described above. Inhibition of mTORC1-mTORC2 resulted in an unsustained

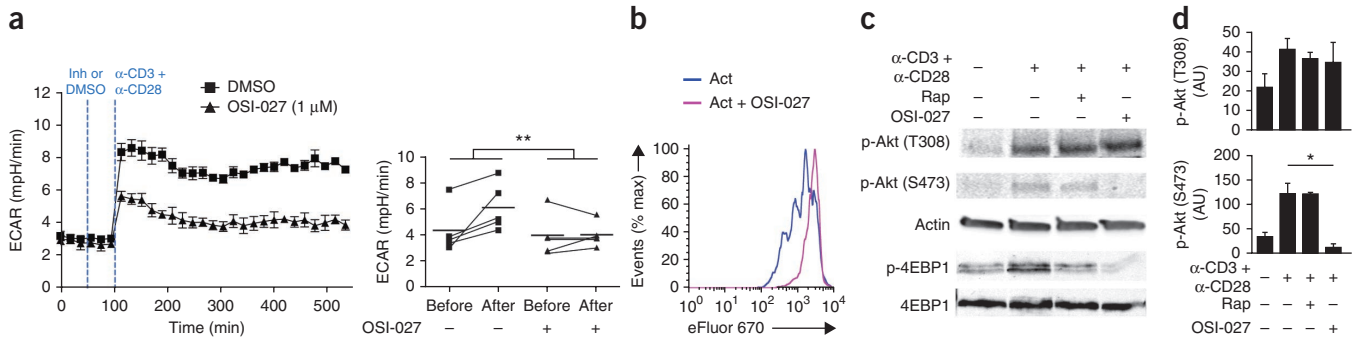

Figure 4 The immediate-early glycolytic switch is dependent on mTORC2 signaling. (**a**) ECAR (left; one of three to five donors) and mean ECAR before and after activation (right; as in **Fig. 2**) of EM CD8$^+$ T cells pretreated with control medium (DMSO) or OSI-027 and then activated with anti-CD3 (1 μg/ml) and anti-CD28 (10 μg/ml). Each symbol (right) represents an individual donor ($n = 5$); small horizontal lines indicate the mean. (**b**) Flow cytometry of EM CD8$^+$ T cells activated with or without pretreatment with OSI-027, as in **a** (presented as in **Fig. 3d**). (**c**) Immunoblot analysis of lysates of EM CD8$^+$ T cells left nonactivated (–) or activated (+) for 3 h with anti-CD3 (2 μg/ml) and anti-CD28 (20 μg/ml) with (+) or without (–) rapamycin (20 ng/ml) or OSI-027 (1 μM), probed for Akt phosphorylated at Thr308 (p-Akt(T308)) or Ser473 (p-Akt(S473)) or total and phosphorylated (p-) 4EBP1; actin serves as a loading control. (**d**) Band intensity for Akt phosphorylated at Thr308 or Ser473 (as in **c**), normalized to actin and presented in arbitrary units ($n = 3$). $^*P < 0.05$ and $^{**}P < 0.01$ (paired two-tailed Student's *t*-test). Data are representative of five (**a**), four (**b**) or three (**d**) experiments (mean and s.e.m. in **a**,**d**) or are from one experiment representative of three separate experiments (**c**; all one experiment per donor).

increase in the ECAR (**Fig. 4a**). Analogous to results obtained with rapamycin, treatment with OSI-027 also blocked cell proliferation (**Fig. 4b**). To investigate the possible effect of OSI-027 on mTORC2 activity, we compared the phosphorylation of Akt at Ser473 or Thr308 in activated EM CD8$^+$ T cells, by immunoblot analyses (**Fig. 4c**,**d**). The phosphorylation of Thr308 and Ser473 was increased after activation of EM CD8$^+$ T cells. Activation of EM cells in the presence of rapamycin or OSI-027 did not affect the abundance of phosphorylated Thr308 (**Fig. 4c**,**d**), which indicated that phosphorylation at Thr308 was not regulated by mTORC1-mTORC2 activity. Treatment with OSI-027 resulted in a lower abundance of phosphorylated Ser473 in activated EM cells, whereas phosphorylation of Ser473 was insensitive to treatment with rapamycin (**Fig. 4c**,**d**). Under identical conditions, we also assessed phosphorylation of 4EBP1 (Thr37-Thr46), a downstream target of mTORC1 (**Fig. 4c**). The phosphorylation of 4EBP1 was increased in EM CD8$^+$ T cells activated with anti-CD3 plus anti-CD28. Inhibition of mTORC1 activity with either rapamycin or OSI-027 led to a lower abundance of phosphorylated 4EBP1. The sensitivity of the immediate-early glycolytic switch to inhibition of mTORC2 indicated that phosphorylation of Akt at Ser473 was critical for this event.

Immediate-early glycolysis supports interferon-γ production

Memory CD8$^+$ T cells have less stringent activation requirements than do naive T cells[13,31]. EM CD8$^+$ T cells contain preformed cytotoxic granules and are able to rapidly upregulate the expression of cytokines such as interferon-γ (IFN-γ) and tumor-necrosis factor[32,33]. IFN-γ synthesis by effector CD8$^+$ T cells has been linked to glucose metabolism[34,35]. Given the rapid upregulation of glycolytic flux in EM CD8$^+$ T cells stimulated with anti-CD3 plus anti-CD28, we assessed the role of the immediate-early glycolytic phase on the activation of CD8$^+$ T cells and elaboration of their effector function. Specifically, we assessed cell-surface expression of the activation marker CD69 and assayed IFN-γ production in quiescent and activated naive and EM CD8$^+$ T cells. Among naive CD8$^+$ T cells, the frequency of CD69-expressing cells increased significantly after activation (**Fig. 5a**). In contrast, IFN-γ remained undetectable after 12 h of stimulation (**Fig. 5b**), which indicated that IFN-γ synthesis in previously unprimed (i.e., naive) human CD8$^+$ T cells required prolonged activation. EM CD8$^+$ T cells also upregulated CD69 expression after activation (**Fig. 5c**). In contrast to IFN-γ production by naive cells, however, IFN-γ production by EM CD8$^+$ T cells was readily detectable 12 h after stimulation (**Fig. 5d**). To determine the role of the Akt-mTORC1 axis in the early activation of EM CD8$^+$ T cells, we treated cells with Akti-1/2 or rapamycin. Surface expression of CD69 remained elevated under both treatment conditions, although the frequency of CD69$^+$ cells was slightly decreased among cells treated with Akti-1/2 (**Fig. 5c**). Inhibition of Akt resulted in much less IFN-γ production by EM CD8$^+$ T cells, whereas treatment with rapamycin had no significant effect on early IFN-γ synthesis (**Fig. 5d**). The dependence of early IFN-γ production on Akt suggested that the immediate-early glycolytic phase probably had a role in this effector response.

To define the dependence of CD69 upregulation and IFN-γ production on glucose availability, we further activated EM CD8$^+$ T cells in a low concentration (0.5 mM) of glucose alone or a low concentration of glucose plus 2-DG or in a normal concentration (10 mM) of glucose. The frequency of CD69$^+$ cells was similar in all conditions (**Fig. 5e**), which demonstrated that early activation of EM CD8$^+$ T cells occurred independently of glucose availability. IFN-γ production was induced similarly with either 10 mM glucose or 0.5 mM glucose (**Fig. 5d**,**f**), which indicated that a low concentration of glucose was sufficient to drive IFN-γ production in EM CD8$^+$ T cells. However, after the addition of 2-DG, IFN-γ production was greatly diminished (**Fig. 5f**). Finally, transient immediate-early glycolysis triggered by stimulation with anti-CD3 alone was able to support limited IFN-γ production[24] (**Supplementary Fig. 8**). However, in the context of sustained glycolytic activity induced through coactivation with anti-CD3 plus anti-CD28, IFN-γ production was increased almost twofold (**Supplementary Fig. 8**). These findings demonstrated that the IFN-γ recall response of EM CD8$^+$ T cells was highly dependent on immediate-early glycolytic flux. Moreover, these experiments correlated Akt activity to IFN-γ production of EM CD8$^+$ T cells, via mediation of an immediate-early glycolytic switch and thus increased glucose metabolism.

Immediate-early glycolysis in central memory T cells

Although EM CD8$^+$ T cells provide a major pool of memory cells able to immediately elaborate effector molecules after reencountering the cognate antigen, rapid IFN-γ production is also detected among central memory (CM) CD8$^+$ T cells[17]. Thus, we compared the

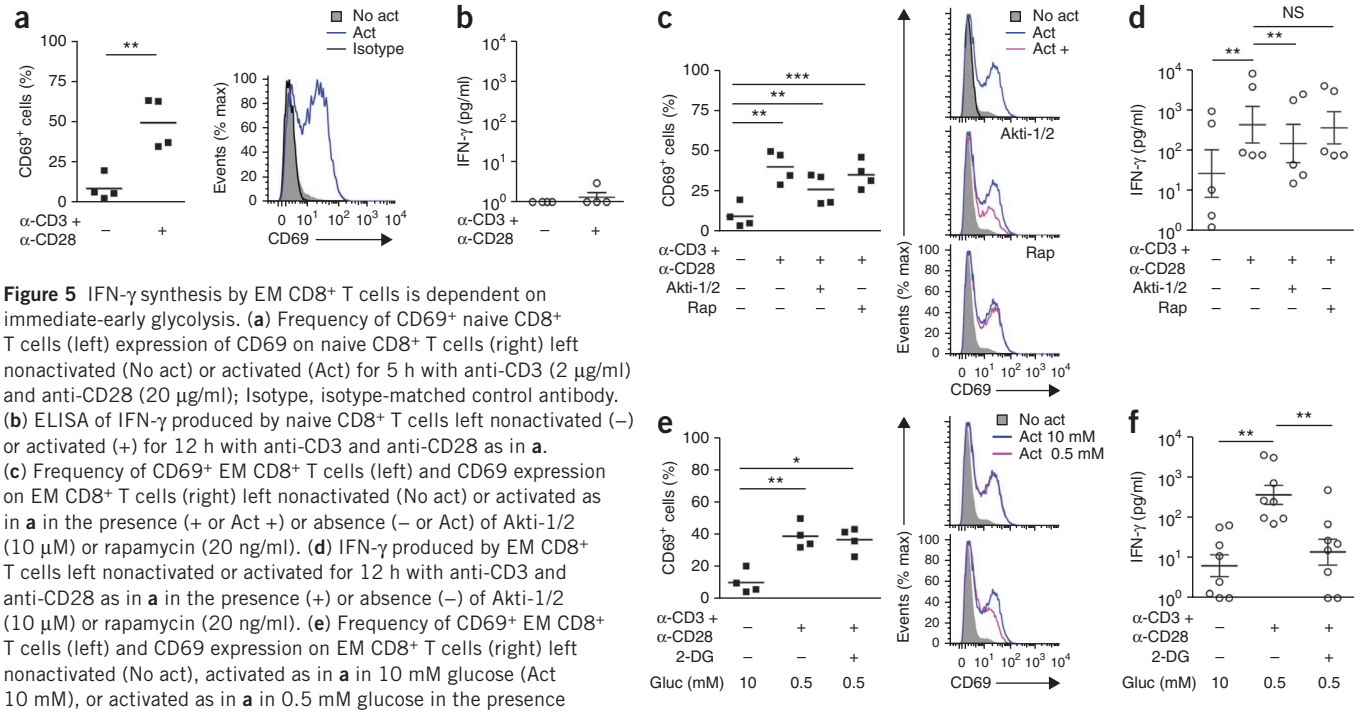

Figure 5 IFN-γ synthesis by EM CD8⁺ T cells is dependent on immediate-early glycolysis. (**a**) Frequency of CD69⁺ naive CD8⁺ T cells (left) expression of CD69 on naive CD8⁺ T cells (right) left nonactivated (No act) or activated (Act) for 5 h with anti-CD3 (2 μg/ml) and anti-CD28 (20 μg/ml); Isotype, isotype-matched control antibody. (**b**) ELISA of IFN-γ produced by naive CD8⁺ T cells left nonactivated (–) or activated (+) for 12 h with anti-CD3 and anti-CD28 as in **a**. (**c**) Frequency of CD69⁺ EM CD8⁺ T cells (left) and CD69 expression on EM CD8⁺ T cells (right) left nonactivated (No act) or activated as in **a** in the presence (+ or Act +) or absence (– or Act) of Akti-1/2 (10 μM) or rapamycin (20 ng/ml). (**d**) IFN-γ produced by EM CD8⁺ T cells left nonactivated or activated for 12 h with anti-CD3 and anti-CD28 as in **a** in the presence (+) or absence (–) of Akti-1/2 (10 μM) or rapamycin (20 ng/ml). (**e**) Frequency of CD69⁺ EM CD8⁺ T cells (left) and CD69 expression on EM CD8⁺ T cells (right) left nonactivated (No act), activated as in **a** in 10 mM glucose (Act 10 mM), or activated as in **a** in 0.5 mM glucose in the presence (Act 0.5 mM; bottom) or absence (Act 0.5 mM; top) of 2-DG. (**f**) IFN-γ in EM CD8⁺ T cells left nonactivated in the presence of 10 mM glucose or activated for 12 h with anti-CD3 and anti-CD28 (as in **d**) in the presence of 0.5 mM glucose or 0.5 mM glucose plus 2-DG ($n = 8$, paired two-tailed Student's *t*-tests). Each symbol represents an individual donor; small horizontal lines indicate the mean (and s.e.m. in **b**,**d**,**f**). $^*P < 0.05$, $^{**}P < 0.01$ and $^{***}P < 0.001$ (paired two-tailed Student's *t*-test (**a**,**c**–**f**)). Data are representative of four (**a**–**c**,**e**), five (**d**) or eight (**f**) experiments (all one experiment per donor).

immediate-early glycolytic switch and glycolysis-dependent IFN-γ production in CM CD8⁺ T cells with that in EM CD8⁺ T cells. In these experiments, we used the lymph node–homing receptor CD62L (rather than the lymph node–homing receptor CCR7), in combination with naive-cell marker CD45RA, as marker for distinguishing CM (CD45RA⁻CD62L⁺) cells from EM (CD45RA⁻CD62L⁻) cells because of the more distinct separation of CM populations versus EM populations (**Supplementary Fig. 1**). We used anti-CD3 plus anti-CD28 to activate CM and EM CD8⁺ T cells and noted identical ECAR profiles for memory subpopulations (**Fig. 6a**–**c**). Likewise, IFN-γ production was diminished in both CM CD8⁺ T cells and EM CD8⁺ T cells after treatment with Akti-1/2 (**Fig. 6d**,**e**). Finally, as observed in EM CD8⁺ T cells, 2-DG also resulted in less IFN-γ production in CM CD8⁺ T cells (data not shown). Immediate-early glycolysis thus is a general feature of memory CD8⁺ T cells.

Glycolysis supports virus-specific CD8⁺ T cell responses

To assess at an antigen-specific level the dependence of rapid IFN-γ production by memory CD8⁺ T cells on glycolysis, we next characterized Epstein-Barr virus (EBV)-specific CD8⁺ T cell responses in EBV-seropositive donors by overnight enzyme-linked immunospot (ELISPOT) assay of IFN-γ. As a 'readout', we calculated the number of spot-forming cells relative to that of input cells, which reflects the overall frequency of detectable peptide-specific responses. We also assessed the surface size and staining intensity of spots, which are a measure of the amount of IFN-γ released per cell[36]. The frequency of spot-forming cells per 1×10^6 input cells was 350 (donor A), 50 (donor B) and 240 (donor C). In the presence of 2-DG, the frequency of EBV-specific responses enhanced by anti-CD28 decreased by 25–100% (**Fig. 7**). In addition, there was also a consistent reduction in the size and staining intensity of EBV-specific responses (**Fig. 7**).

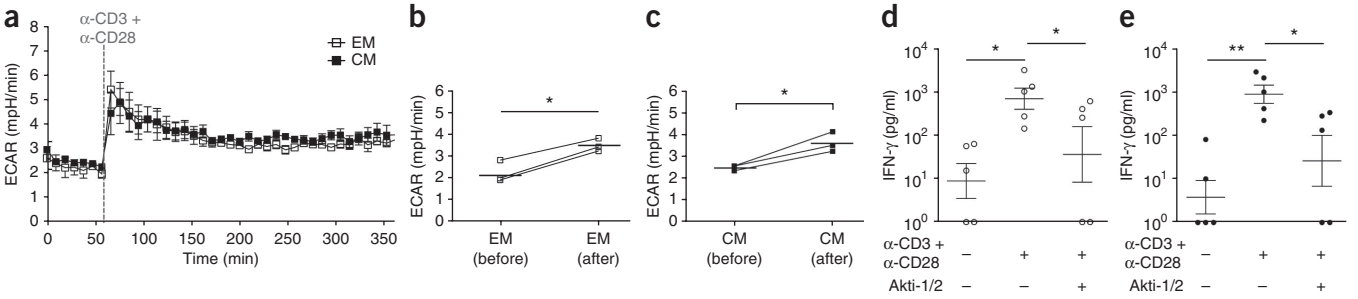

Figure 6 The immediate-early glycolytic switch is a common feature of memory CD8⁺ T cell subpopulations. (**a**) Combined ECAR of EM and CM CD8⁺ T cells after 'in-Seahorse' activation with anti-CD3 (1 μg/ml) and anti-CD28 (10 μg/ml). (**b**,**c**) Mean ECAR of EM CD8⁺ T cells (**b**) and CM CD8⁺ T cells (**c**) before and after injection (as in **Fig. 2**). (**d**,**e**) ELISA of IFN-γ in EM CD8⁺ T cells (**d**) and CM CD8⁺ T cells (**e**) left nonactivated or activated for 12 h with anti-CD3 (2 μg/ml) and anti-CD28 (20 μg/ml) in the presence or absence of Akti-1/2 (10 μM). $^*P < 0.05$, $^{**}P < 0.01$ (paired two-tailed Student's *t*-test (**c**–**e**). Each symbol represents an individual donor; small horizontal lines indicate the mean (and s.e.m. in **d**,**e**). Data are representative of three experiments with results pooled from three donors (**a**; error bars, s.e.m.) or three experiments (**b**,**c**) or five (**d**,**e**) experiments (all one experiment per donor).

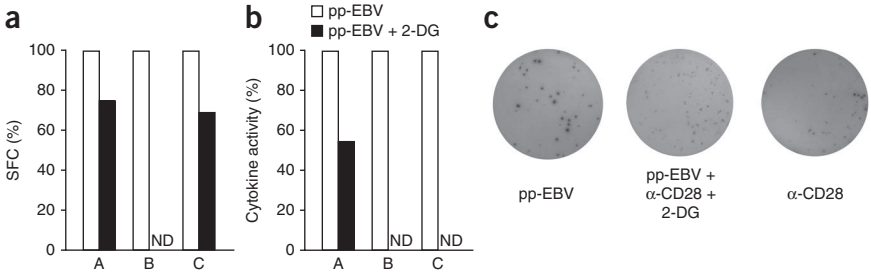

Figure 7 IFN-γ production by EBV-specific memory CD8⁺ T cells is diminished in the presence of 2-DG. (**a**) ELISPOT assay of the frequency of IFN-γ⁺ EBV-specific CD8⁺ T cells among peripheral blood mononuclear cells obtained from EBV-seropositive donors ($n = 3$ (A–C)) and stimulated with pooled HLA-I-restricted EBV peptides alone (pp-EBV) or with EBV peptides and anti-CD28 in the presence of 2-DG (pp-EBV + 2-DG), presented as spot-forming cells (SFC), relative to results obtained by stimulation with EBV peptides alone, set as 100%. ND, not detected. (**b**) Cytokine activity (indicative of the amount of IFN-γ release) of cells (from donors A–C) stimulated with the EBV peptides as in **a** in the presence of 2-DG (with costimulation by anti-CD28), determined by combined analysis of spot surface size and staining intensity and presented relative to that of cells stimulated with the EBV peptides alone, set as 100%. (**c**) Wells of reactions induced by EBV peptides alone (left), EBV peptides plus 2-DG with costimulation with anti-CD28 (middle) or anti-CD28 alone (control; right). Data are representative of three experiments (all one experiment per donor).

These experiments established the dependence of cognate, EBV-specific memory responses on immediate-early glycolysis.

Chromatin remodeling and immediate-early glycolysis

The rapid production of IFN-γ by EM naive CD8⁺ T cells but not by naive CD8⁺ T cells suggested differences in epigenetic regulation of the *IFNG* promoter. Increased glycolytic activity in proliferating cells decreases the cellular ratio of NAD^+ to NADH, which can affect epigenetic modifications, such as deacetylation mediated by NAD^+-sensitive class III histone deacetylases[12,37]. To determine the effect of immediate-early glycolysis on NAD^+/NADH, we assessed the concentration of NAD^+ and NADH in unstimulated EM CD8⁺ T cells and those activated with anti-CD3 plus anti-CD28. At 6 h after activation, there was only a small yet significant increase in NAD^+ concentration in EM CD8⁺ T cells (**Fig. 8a**). Notably, NADH concentrations were very low or undetectable under nonactivating and immediate-early–activating conditions (**Fig. 8a**). We detected substantial changes in the total NADH concentration and in NAD^+/NADH only in actively proliferating CD8⁺ T cells (**Fig. 8a**) and in proliferating Jurkat human T lymphocytes (data not shown). Despite the small increase in NAD^+ early after activation, EM CD8⁺ T cells rapidly produced IFN-γ in a glycolysis-dependent manner (**Fig. 5f**). Hence, the small increase in NAD^+ did not seem to have a functionally relevant effect on *IFNG* transcription. These findings also demonstrated that NAD^+/NADH in resting and nascently activated EM CD8⁺ T cells favored NAD^+, which emphasized a difference in the bioenergetic status of immediate-early activated CD8⁺ T cells and that of proliferating CD8⁺ T cells.

Histones are modified differently in the *IFNG* promoter in naive versus memory CD8⁺ T cells[38,39]. Specifically, hyperacetylation of histone H3 Lys9 (H3K9) in the *IFNG* promoter of memory CD8⁺ T cells reflects an active chromatin conformation state[38]. Additionally, in mouse CD8⁺ T cells, substantial chromatin remodeling (i.e., histone loss) takes place in the promoters of *Gzmb* (which encodes granzyme B) and *Ifng* after activation, which facilitates binding of RNA polymerase II and gene expression[40,41]. It is well established that glycolysis provides substrates for histone acetylation[42]; however, its effect on chromatin remodeling remains undefined. To determine the effect of immediate-early glycolysis on histone loss and modification in the *IFNG* promoter of nascently activated memory CD8⁺ T cells, we assessed total histone H3 and acetylated H3K9 in proximal and distal regions of the promoter (positions −7, −382 and −4179 relative to the transcription start site) after activation. We observed a substantial loss of histone H3, indicative of rapid chromatin remodeling, in all three regions of the *IFNG* promoter in both naive and EM CD8⁺ T cells after 6 h of stimulation with anti-CD3 plus anti-CD28 (**Fig. 8b**). In the presence of 2-DG, loss of histone H3 at the *IFNG* promoter was abrogated in activated EM CD8⁺ T cells (**Fig. 8b**), which indicated a role for immediate-early glycolysis in chromatin remodeling. Under nonactivating conditions, there was a greater abundance of acetylated H3K9 in all three *IFNG* promoter regions in EM CD8⁺ T cells than in naive CD8⁺ T cells (**Fig. 8b**), reflective of the active state of *IFNG* promoters in memory CD8⁺ T cells[38,39]. After activation, there was a marked decrease in detectable acetylated H3K9 in the *IFNG* promoter of both subpopulations (**Fig. 8b**). The observed loss of acetylated

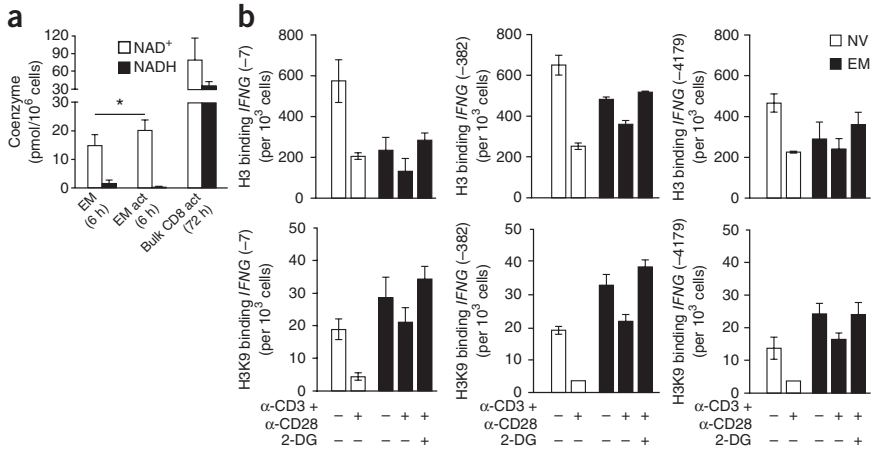

Figure 8 Chromatin remodeling of the *IFNG* promoter in EM CD8⁺ T cells. (**a**) NAD^+ and NADH in EM CD8⁺ T cells ($n = 5$ donors) cultured for 6 h under nonstimulating conditions (left) or stimulated with anti-CD3 plus anti-CD28 (middle) or in bulk CD8⁺ T cells ($n = 3$ donors) activated for 72 h (right). $^*P < 0.05$ (paired two-tailed Student's *t*-test). (**b**) Chromatin-immunoprecipitation analysis of naive and EM CD8⁺ T cells left unstimulated or activated for 6 h with anti-CD3 plus anti-CD28 in the presence or absence of 50 mM 2-DG, assessing the binding of histone H3 (top) or acetylated H3K9 (bottom) to the various regions of the *IFNG* promoter (vertical axes). Data are representative of five experiments (**a**; one donor per experiment; error bars, s.e.m.) or one experiment with cells pooled from three donors (**b**; error bars, s.d.).

histone H3 was in agreement with the lower total histone H3 content at the *IFNG* promoter of activated CD8$^+$ T cells. Notably, the abundance of acetylated H3K9 remained higher in activated EM CD8$^+$ T cells than in their activated naive counterparts (**Fig. 8b**), which indicated that the *IFNG* promoter of activated EM CD8$^+$ T cells maintained an active chromatin conformation state. Finally, similar to the effect of 2-DG on histone H3 content, the abundance of acetylated H3K9 in EM CD8$^+$ T cells activated in the presence of 2-DG was similar to that of nonactivated control cells (**Fig. 8b**), which again indicated the importance of immediate-early glycolysis in regulating the positioning of histone H3 in the *IFNG* promoter of activated memory CD8$^+$ T cells. Together these findings indicated that the diminished IFN-γ synthesis in EM CD8$^+$ T cells after blockade of immediate-early glycolysis was linked to the abrogation of chromatin remodeling in the *IFNG* promoter region and not to lower abundance of acetylated H3K9.

DISCUSSION

A defining metabolic feature of EM CD8$^+$ T cells was their selective ability to immediately upregulate and sustain aerobic glycolysis after mitochondrial stress. EM CD8$^+$ T cells migrate to and reside in various environmental niches[15–17]. Thus, a high glycolytic capacity probably affords increased adaptability to changes in nutrient availability and/or stimulatory conditions. Glycolysis was also increased in memory CD8$^+$ T cells after stimulation via the TCR plus CD28 and activation of the PI(3)K-Akt pathway. That Akt-dependent, immediate-early glycolytic phase was critical for rapid IFN-γ production by memory CD8$^+$ T cells. Pharmacological blockade of glycolysis during the early phase of activation with anti-CD3 plus anti-CD28 resulted in the diminution of IFN-γ production by EM CD8$^+$ T cells, potentially via abrogation of chromatin remodeling.

The abundance of key glycolytic enzymes (HK1, GAPDH, PKM2 and LDHA) was similar in the naive and EM CD8$^+$ T cell subsets. The isoenzyme PKM2, which is typically found in highly proliferating tumor cells[43], was expressed in both naive CD8$^+$ T cells and EM CD8$^+$ T cells. This is in agreement with a published report showing the presence of PKM2 in quiescent mouse T cells[11]. PKM2 can occur in tetrameric or dimeric form, with the former structure being associated with increased degradation of glucose into lactate and the latter structure being associated with the accumulation of glycolytic intermediates used by rapidly dividing cells[43]. How PK structure is regulated in naive and EM CD8$^+$ T cells after stimulation mediated by the TCR plus CD28 remains to be defined. GAPDH activity was greater in EM CD8$^+$ T cells than in their naive counterparts. Notably, GAPDH in naive cells was located mainly in the nucleus. In EM cells, we detected GAPDH in nuclear and cytoplasmic compartments, and cytoplasmic GAPDH expression was enhanced after stimulation mediated by the TCR plus CD28. Moreover, inhibition of GAPDH activity abolished the immediate-early glycolytic switch in EM CD8$^+$ T cells. Thus, the increased abundance of cytoplasmic GAPDH in EM CD8$^+$ T cells under quiescent and activating conditions could be linked to their higher glycolytic capacity. Notably, the activity of PK and GAPDH is subject to regulation at various levels (including post-translational modifications, oligomerization state of enzymes and allosteric regulation). How differences in enzymatic regulation affect glycolytic capacity and T cell functionality remains to be investigated further.

T cell activation is dependent mainly on stimulation via the TCR and CD28. Costimulation through CD28 via its ligands CD80 or CD86 results in activation of the PI(3)K-Akt pathway and upregulation of cell-surface expression of the Glut1 glucose transporter[6,7]. Costimulation via CD28 is also important for the reexpansion of memory CD8$^+$ T cell populations by promoting cell-cycle progression[44]. Moreover, mice lacking CD80 and CD86 show deficits in memory CD8$^+$ T cell recall responses[45]. Our data indicated that memory CD8$^+$ T cells relied on CD28 signaling to sustain the immediate-early metabolic switch and that costimulation via CD28 was also important for enhanced IFN-γ production. The activity of Akt and its phosphorylation by the upstream kinases PI(3)K (phosphorylation of Akt at Thr308) and mTORC2 (phosphorylation of Akt at Ser473) were required for a stable metabolic switch and for cytoplasmic expression of GAPDH. Of note, phosphorylation of Akt at Ser473 by mTORC2 is essential for enhancing glycolytic activity in hepatocytes by enhancing expression of the hexokinase isoenzyme glucokinase[46]. It remains to be determined whether activation of Akt in memory T cells has similar effects on regulating the expression of hexokinase isoenzymes. Akt also regulates the surface expression of glucose transporters by phosphorylating the Rab-GTPase–activating proteins AS160 and TBC1D1 (ref. 47). AS160 transcripts are more abundant in T cells from patients with atopic dermatitis than in those from healthy controls[48]. Thus, dysregulation of Akt-mediated glucose transport in T cells could potentially lead to a loss of peripheral tolerance.

GAPDH blocks IFN-γ production by binding to mRNA encoding IFN-γ[35]. Here we found that the CD28-mediated immediate-early glycolytic switch enhanced rapid IFN-γ production by human EM CD8$^+$ T cells, potentially via histone remodeling of the *IFNG* promoter. Given the role of glycolysis in epigenetic regulation[49], future studies should elucidate the specific mechanism by which immediate-early glycolytic flux affects remodeling of the *IFNG* promoter in EM CD8$^+$ T cells. Together these findings assign to the Warburg effect an added role beyond supporting the proliferation of effector T cells; that is, in regulating the immediate-early effector response of memory CD8$^+$ T cells.

METHODS

Methods and any associated references are available in the online version of the paper.

Note: Any Supplementary Information and Source Data files are available in the online version of the paper.

ACKNOWLEDGMENTS

We thank E. Palmer and J.A. Schifferli for discussion of data; E. Traunecker and T. Krebs for technical support with cell sorting; B. Erne for help with imaging; A. Buser (University Hospital Basel) for buffy coats; and M. Stern for statistical help. Supported by the Swiss National Science Foundation (31003A_135677 to C.H., 323630-128881 to P.M.G. and 323530-139181 to M.F.) and Roche (S.D.).

AUTHOR CONTRIBUTIONS

P.M.G. designed, did and analyzed most experiments; G.R.B. designed, did and analyzed experiments and helped write the manuscript; L.R., M.F., S.D., A.J., B.D. and G.H. designed, did and analyzed experiments; and C.H. initiated and oversaw the study, analyzed data and wrote the manuscript.

COMPETING FINANCIAL INTERESTS

The authors declare no competing financial interests.

1. Haring, J.S., Badovinac, V.P. & Harty, J.T. Inflaming the CD8$^+$ T cell response. *Immunity* **25**, 19–29 (2006).
2. Kaech, S.M. & Wherry, E.J. Heterogeneity and cell-fate decisions in effector and memory CD8$^+$ T cell differentiation during viral infection. *Immunity* **27**, 393–405 (2007).
3. Fox, C.J., Hammerman, P.S. & Thompson, C.B. Fuel feeds function: energy metabolism and the T-cell response. *Nat. Rev. Immunol.* **5**, 844–852 (2005).
4. Plas, D.R., Rathmell, J.C. & Thompson, C.B. Homeostatic control of lymphocyte survival: potential origins and implications. *Nat. Immunol.* **3**, 515–521 (2002).

5. Frauwirth, K.A. & Thompson, C.B. Regulation of T lymphocyte metabolism. *J. Immunol.* **172**, 4661–4665 (2004).
6. Frauwirth, K.A. *et al.* The CD28 signaling pathway regulates glucose metabolism. *Immunity* **16**, 769–777 (2002).
7. Jacobs, S.R. *et al.* Glucose uptake is limiting in T cell activation and requires CD28-mediated Akt-dependent and independent pathways. *J. Immunol.* **180**, 4476–4486 (2008).
8. Greiner, E.F., Guppy, M. & Brand, K. Glucose is essential for proliferation and the glycolytic enzyme induction that provokes a transition to glycolytic energy production. *J. Biol. Chem.* **269**, 31484–31490 (1994).
9. Maciver, N.J. *et al.* Glucose metabolism in lymphocytes is a regulated process with significant effects on immune cell function and survival. *J. Leukoc. Biol.* **84**, 949–957 (2008).
10. Board, M., Humm, S. & Newsholme, E.A. Maximum activities of key enzymes of glycolysis, glutaminolysis, pentose phosphate pathway and tricarboxylic acid cycle in normal, neoplastic and suppressed cells. *Biochem. J.* **265**, 503–509 (1990).
11. Wang, R. *et al.* The transcription factor Myc controls metabolic reprogramming upon T lymphocyte activation. *Immunity* **35**, 871–882 (2011).
12. Lunt, S.Y. & Vander Heiden, M.G. Aerobic glycolysis: meeting the metabolic requirements of cell proliferation. *Annu. Rev. Cell Dev. Biol.* **27**, 441–464 (2011).
13. Masopust, D. & Picker, L.J. Hidden memories: frontline memory T cells and early pathogen interception. *J. Immunol.* **188**, 5811–5817 (2012).
14. Geginat, J., Lanzavecchia, A. & Sallusto, F. Proliferation and differentiation potential of human CD8$^+$ memory T-cell subsets in response to antigen or homeostatic cytokines. *Blood* **101**, 4260–4266 (2003).
15. Klonowski, K.D. *et al.* Dynamics of blood-borne CD8 memory T cell migration *in vivo*. *Immunity* **20**, 551–562 (2004).
16. Masopust, D., Vezys, V., Marzo, A.L. & Lefrancois, L. Preferential localization of effector memory cells in nonlymphoid tissue. *Science* **291**, 2413–2417 (2001).
17. Sathaliyawala, T. *et al.* Distribution and compartmentalization of human circulating and tissue-resident memory T cell subsets. *Immunity* **38**, 187–197 (2013).
18. Wu, M. *et al.* Multiparameter metabolic analysis reveals a close link between attenuated mitochondrial bioenergetic function and enhanced glycolysis dependency in human tumor cells. *Am. J. Physiol. Cell Physiol.* **292**, C125–C136 (2007).
19. van der Windt, G.J. *et al.* Mitochondrial respiratory capacity is a critical regulator of CD8$^+$ T cell memory development. *Immunity* **36**, 68–78 (2012).
20. Sirover, M.A. Subcellular dynamics of multifunctional protein regulation: mechanisms of GAPDH intracellular translocation. *J. Cell. Biochem.* **113**, 2193–2200 (2012).
21. Mazzola, J.L. & Sirover, M.A. Subcellular localization of human glyceraldehyde-3-phosphate dehydrogenase is independent of its glycolytic function. *Biochim. Biophys. Acta* **1622**, 50–56 (2003).
22. Dziurla, R. *et al.* Effects of hypoxia and/or lack of glucose on cellular energy metabolism and cytokine production in stimulated human CD4$^+$ T lymphocytes. *Immunol. Lett.* **131**, 97–105 (2010).
23. Kusner, L.L., Sarthy, V.P. & Mohr, S. Nuclear translocation of glyceraldehyde-3-phosphate dehydrogenase: a role in high glucose-induced apoptosis in retinal Muller cells. *Invest. Ophthalmol. Vis. Sci.* **45**, 1553–1561 (2004).
24. Soond, D.R. *et al.* PI3K p110δ regulates T-cell cytokine production during primary and secondary immune responses in mice and humans. *Blood* **115**, 2203–2213 (2010).
25. Brunn, G.J. *et al.* Direct inhibition of the signaling functions of the mammalian target of rapamycin by the phosphoinositide 3-kinase inhibitors, wortmannin and LY294002. *EMBO J.* **15**, 5256–5267 (1996).
26. Finlay, D.K. *et al.* PDK1 regulation of mTOR and hypoxia-inducible factor 1 integrate metabolism and migration of CD8$^+$ T cells. *J. Exp. Med.* **209**, 2441–2453 (2012).
27. Shi, L.Z. *et al.* HIF1α-dependent glycolytic pathway orchestrates a metabolic checkpoint for the differentiation of TH17 and Treg cells. *J. Exp. Med.* **208**, 1367–1376 (2011).
28. Guertin, D.A. *et al.* Ablation in mice of the mTORC components raptor, rictor, or mLST8 reveals that mTORC2 is required for signaling to Akt-FOXO and PKCα, but not S6K1. *Dev. Cell* **11**, 859–871 (2006).
29. Gan, X., Wang, J., Su, B. & Wu, D. Evidence for direct activation of mTORC2 kinase activity by phosphatidylinositol 3,4,5-trisphosphate. *J. Biol. Chem.* **286**, 10998–11002 (2011).
30. Bhagwat, S.V. *et al.* Preclinical characterization of OSI-027, a potent and selective inhibitor of mTORC1 and mTORC2: distinct from rapamycin. *Mol. Cancer Ther.* **10**, 1394–1406 (2011).
31. Jameson, S.C. & Masopust, D. Diversity in T cell memory: an embarrassment of riches. *Immunity* **31**, 859–871 (2009).
32. Hansen, S.G. *et al.* Effector memory T cell responses are associated with protection of rhesus monkeys from mucosal simian immunodeficiency virus challenge. *Nat. Med.* **15**, 293–299 (2009).
33. Harari, A., Enders, F.B., Cellerai, C., Bart, P.A. & Pantaleo, G. Distinct profiles of cytotoxic granules in memory CD8 T cells correlate with function, differentiation stage, and antigen exposure. *J. Virol.* **83**, 2862–2871 (2009).
34. Cham, C.M. & Gajewski, T.F. Glucose availability regulates IFN-γ production and p70S6 kinase activation in CD8$^+$ effector T cells. *J. Immunol.* **174**, 4670–4677 (2005).
35. Chang, C.H. *et al.* Posttranscriptional control of T cell effector function by aerobic glycolysis. *Cell* **153**, 1239–1251 (2013).
36. Helms, T. *et al.* Direct visualization of cytokine-producing recall antigen-specific CD4 memory T cells in healthy individuals and HIV patients. *J. Immunol.* **164**, 3723–3732 (2000).
37. Kong, S., McBurney, M.W. & Fang, D. Sirtuin 1 in immune regulation and autoimmunity. *Immunol. Cell Biol.* **90**, 6–13 (2012).
38. Fann, M. *et al.* Histone acetylation is associated with differential gene expression in the rapid and robust memory CD8$^+$ T-cell response. *Blood* **108**, 3363–3370 (2006).
39. Weng, N.P., Araki, Y. & Subedi, K. The molecular basis of the memory T cell response: differential gene expression and its epigenetic regulation. *Nat. Rev. Immunol.* **12**, 306–315 (2012).
40. Juelich, T. *et al.* Interplay between chromatin remodeling and epigenetic changes during lineage-specific commitment to granzyme B expression. *J. Immunol.* **183**, 7063–7072 (2009).
41. Zediak, V.P., Johnnidis, J.B., Wherry, E.J. & Berger, S.L. Cutting edge: persistently open chromatin at effector gene loci in resting memory CD8$^+$ T cells independent of transcriptional status. *J. Immunol.* **186**, 2705–2709 (2011).
42. Wellen, K.E. *et al.* ATP-citrate lyase links cellular metabolism to histone acetylation. *Science* **324**, 1076–1080 (2009).
43. Mazurek, S. Pyruvate kinase type M2: a key regulator of the metabolic budget system in tumor cells. *Int. J. Biochem. Cell Biol.* **43**, 969–980 (2011).
44. Borowski, A.B. *et al.* Memory CD8$^+$ T cells require CD28 costimulation. *J. Immunol.* **179**, 6494–6503 (2007).
45. Grujic, M. *et al.* The role of CD80/CD86 in generation and maintenance of functional virus-specific CD8$^+$ T cells in mice infected with lymphocytic choriomeningitis virus. *J. Immunol.* **185**, 1730–1743 (2010).
46. Hagiwara, A. *et al.* Hepatic mTORC2 activates glycolysis and lipogenesis through Akt, glucokinase, and SREBP1c. *Cell Metab.* **15**, 725–738 (2012).
47. Sakamoto, K. & Holman, G.D. Emerging role for AS160/TBC1D4 and TBC1D1 in the regulation of GLUT4 traffic. *Am. J. Physiol. Endocrinol. Metab.* **295**, E29–E37 (2008).
48. Matsumoto, Y. *et al.* Upregulation of the transcript level of GTPase activating protein KIAA0603 in T cells from patients with atopic dermatitis. *FEBS Lett.* **572**, 135–140 (2004).
49. Lu, C. & Thompson, C.B. Metabolic regulation of epigenetics. *Cell Metab.* **16**, 9–17 (2012).

ONLINE METHODS

Isolation of peripheral blood mononuclear cells and CD8$^+$ T cells. Blood samples were obtained from healthy donors after written informed consent was provided. The study was approved by the Swiss Red Cross (blood transfusion service). Peripheral blood mononuclear cells were isolated by standard density-gradient centrifugation protocols (Lymphoprep; Fresenius Kabi). CD8$^+$ T cells were positively selected with MACS beads (Miltenyi Biotec).

Cell sorting. For isolation of naive and EM subsets, positively selected CD8$^+$ T cells were incubated with allophycocyanin-conjugated anti-CCR7 (FABP197; R&D Systems) and Pacific blue–conjugated anti-CD45RA (2H4; Beckman Coulter). CCR7$^+$CD45RA$^+$ (naive) and CCR7$^-$CD45RA$^-$ (EM) subsets were then sorted with a FACSVantage SEM System (BD Bioscience) (**Supplementary Fig. 1a–c**). For isolation of CM and EM subsets, positively selected CD8$^+$ T cells were incubated with allophycocyanin-conjugated anti-CD62L (LT-TD180; ImmunoTools) and Pacific blue–conjugated anti-CD45RA. CD62L$^+$CD45RA$^-$ (CM) and CD62L$^-$CD45RA$^-$ (EM) subsets were sorted with a FACSVantage SEM System (BD Bioscience) (**Supplementary Fig. 1d–f**). Sorted cells were allowed to 'rest' for 3 h in RPMI-1640 medium (Sigma-Aldrich) containing 10% human AB serum (Invitrogen), 50 U/ml penicillin (Invitrogen) and 50 μg/ml streptomycin (Invitrogen) before further analysis.

Flow cytometry. For staining, cells were resuspended in flow cytometry buffer (1% BSA in PBS) and were incubated for 30 min in the dark at 4 °C with the following antibodies: anti-CD45RA (2H4), anti-CCR7 (FABP197), anti-CD62L (LT-TD180), anti-CD69 (FN50; Immunotools) and mouse IgG1 isotype-matched mAb (P3.6.2.8.1; eBioscience). Data were acquired with a FACSCalibur flow cytometer (Becton Dickinson) and were analyzed with FlowJo 8.8.7 software (Tree Star).

OCR and ECAR measurements. For analysis of the OCR (in pmol/min) and ECAR (in mpH/min), the Seahorse XF-24 metabolic extracellular flux analyzer was used (Seahorse Bioscience). CD8$^+$ T cells were resuspended in serum-free unbuffered RPMI-1640 medium (Sigma-Aldrich) and were plated onto Seahorse cell plates (6×10^5 cells per well) coated with Cell-Tak (BD Bioscience) to enhance T cell attachment. Perturbation profiling of the use of metabolic pathways by CD8$^+$ T cells was achieved by the addition of oligomycin (1 μM), 2,4–dinitrophenol (170 μM) and rotenone (1 μM; all from Sigma-Aldrich). Experiments with the Seahorse system were done with the following assay conditions: 2 min mixture; 2 minutes wait; and 4–5 min measurement. Metabolic parameters were then calculated (**Supplementary Fig. 2**).

Confocal microscopy. Fixed cells were viewed and imaged with an LSM 710 confocal microscope (Carl Zeiss) with a 100× oil-immersion objective. Freshly sorted CD8$^+$ T cells subsets were allowed to attach by gravity for 20 min onto culture slides (BD Bioscience) coated with poly-D-lysine. Attached cells were fixed with 4% paraformaldehyde and permeabilized with 0.3% Triton X-100. Cells were stained with anti-GAPDH (D16H11; Cell Signaling Technology) and DAPI (4,6-diamidino-2-phenylindol) for nuclear staining. Stacked images were then collected at intervals of 0.5 or 1 μm. For analysis of the cytoplasmic localization of GAPDH, binary images of the nuclear stain was used as the mask, and fluorescence intensity of cytoplasmic GAPDH of individual cells was quantified. All images were processed with ImageJ software (US National Institutes of Health). All imaging complies with the Nature Publishing policy for image integrity.

'In-Seahorse' T cell activation. To monitor CD8$^+$ T cell activation by metabolic flux analysis (i.e., in real time), anti-CD3 (HIT3a, Biolegend) and anti-CD28 (CD28.2; Biolegend) were directly applied onto plated cells via the instrument's multi-injection ports. Various antibody concentrations were used (figure legends). Both antibodies were injected 60 min after the experiment was initiated. The ECAR and OCR of naive and EM CD8$^+$ T cells were recorded for the duration of the experiment. Mean ECAR before and after antibody injection was used to describe the effects of both antibodies on the glycolysis of CD8$^+$ T cells. Isotype-matched control mAb (IgG2aκ; Biolegend) was used to control for nonspecific effects of anti-CD3. For glucose-free Seahorse experiments, unbuffered glucose-free RPMI-1640 medium (Sigma-Aldrich) was used. For inhibitor experiments, iodoacetate (Sigma-Aldrich), *R*-(−)-deprenyl hydrochloride (Sigma-Aldrich), heptelidic acid (AdipoGen), LY294002 (Sigma-Aldrich), Akti-1/2 (Sigma-Aldrich), rapamycin (Merck KGaA) or 2-deoxy-D-glucose (Sigma-Aldrich) was injected.

Immunoblot analysis. Freshly sorted cells were lysed in RIPA buffer (Thermo Scientific) and protein concentration determined with a BCA protein assay kit (Thermo Scientific). Whole-cell lysates were separated by 4–20% SDS-PAGE and were transferred to nitrocellulose or PVDF membranes. Membranes were probed with anti-HK1 (C35C4), anti-LDHA (C4B5), anti-PKM2 (D78A4), antibody to Akt phosphorylated at Thr308 (C31E5E), antibody to Akt phosphorylated at Ser473 (D9E), anti-4EBP1 (53H11), antibody to phosphorylated 4EBP1 (236B4) and anti-GAPDH (D16H11; all from Cell Signaling Technologies). Blots were then stained with the appropriate secondary antibody (IRDye 800CW–conjugated goat polyclonal antibody to rabbit IgG (926-32211) and IRDye 680RD–conjugated goat polyclonal antibody to mouse IgG (926-68070); both from LI-COR). The Odyssey imaging system (LICOR) was used for detection.

GAPDH, PK and NAD$^+$/NADH assays. For analysis of the activity of GAPDH and PK in CD8$^+$ T cells, assay kits for GAPDH activity (Innoprot) and PK activity (Biovision) were used. For each assay, naive and EM CD8$^+$ T cells (5×10^5 each) were lysed with the lysis buffers provided with each kit and then were processed according to the manufacturer's instructions. The ratio of the concentration NAD$^+$ to that of NADH was determined with an NAD$^+$/NADH colorimetric quantitation kit (Biovision). Nonactivated EM CD8$^+$ T cells (5×10^6) and EM CD8$^+$ T cells (1×10^6) activated for 6 h with anti-CD3 (2 μg/ml) plus anti-CD28 (20 μg/ml) or bulk CD8$^+$ T cells activated for 72 h with anti-CD3 (2 μg/ml) plus anti-CD28 (20 μg/ml) were processed according to the manufacturer's instructions (Biovision).

Lactate measurements. Freshly sorted cells were seeded into U-bottomed 96-well plates (2.4×10^5 cells per well) in glucose-free RPMI-1640 medium (Invitrogen). Each well was supplemented with glucose and inhibitors, followed by activation of cells with soluble anti-CD3 (2 μg/ml) and anti-CD28 (20 μg/ml). Unstimulated cells were included as controls. Lactate concentrations were measured with a Lactate Assay Kit (BioVision).

Proliferation. Sorted cells were labeled with the cell-proliferation dye eFluor670 (eBioscience) at a final concentration of 2.5 μM and were seeded into U-bottomed 96-well plates (1.7×10^5 cells per well). Plated cells were then activated with anti-CD3 (2 μg/ml) and anti-CD28 (20 μg/ml) in serum-free RPMI-1640 medium. Human AB serum was added at 3 h after activation. Proliferation was measured 3 d after activation with a CYAN-ADP flow cytometer (Beckman Coulter).

ELISA of IFN-γ and CD69 expression. Sorted cells were plated into U-bottomed 96-well plates (3×10^5 cells per well) with glucose-free RPMI medium. For inhibitor experiments, cells were cultured inRPMI medium (10% AB serum), then were treated with Akti-1/2 (10 μM) or rapamycin (20 ng/ml). For glucose-dependence experiments, plated cells were first resuspended in glucose-free RPMI medium and then were plated as described above. For inhibition of glucose use, wells were treated with 10 mM 2-DG (Sigma-Aldrich). Plated cells were activated with anti-CD3 (2 μg/ml) and anti-CD28 (20 μg/ml) and, at 3 h after activation, undialyzed human AB serum (final concentration, 10%; approximately 0.5 mM glucose) was added to each well. For assessment of CD69 expression, cells were activated for 5 h and stained with phycoerythrin-conjugated anti-CD69 or the appropriate isotype-matched control mAb. Concentrations of human IFN-γ were measured in supernatants at 12 h after activation with an IFN-γ ELISA kit (eBioscience).

IFN-γ ELISPOT. Virus-specific IFN-γ production was determined by ELISPOT analysis as described[50]. 96-well HTS ELISPOT plates from Millipore (Merck) were precoated overnight with 5 μg/ml of anti-IFN-γ (1-DIK; Mabtech) and were washed with sterile PBS containing 1% FCS before use. After plates were washed, R10 culture medium was added (30 μl per well) to avoid drying of the membrane, and cells were then added (1×10^5 per well in 100 μl of R10) in presence or absence of 50 mM 2-DG and anti-CD28 (20 μg/ml). The EBV-specific CD8$^+$ T cell response was assessed; a set of peptides consisting of

91 HLA I-restricted optimal epitopes was the source of antigen. Peptides (all synthesized at Massachusetts General Hospital) were titrated for optimal response and were added at a final concentration of 0.2 μg/ml. *Staphylococcus aureus* enterotoxin B (Sigma-Aldrich) was added at a concentration of 0.07 μg/well to serve as positive control. Plates were incubated for 14 h at 37 °C with 5% CO_2 before being developed. After plates were washed with PBS, 100 μl of biotinylated anti-IFN-γ (1 μg/ml; 7-B6–1; Mabtech) was added and plates were incubated for 2 h at 20–24 °C. Plates were washed again and then incubated for 1 h at 20–24 °C in the dark with streptavidin-coupled alkaline phosphatase (1:1,000 dilution; Streptavidin-ALP-PQ; Mabtech). After further washing, IFN-γ production was detected as spots after 7 min of incubation with BCIP-NBT (Mabtech). The color reaction was stopped by washing of the plates, and plates were air-dried before analysis with an AID ELISPOT Reader Unit (Autoimmun Diagnostika; AID Diagnostika). Results are presented as spot-forming cells per 1×10^6 input cells, and cytokine activity per well (surface × intensity of spots per well, determined application of a predefined algorithm (180 (size), 40 (intensity), 1 (gradient)) according to the manufacturer's information). Thresholds for positive responses were determined as the mean plus three standard deviations of negative control wells. Images of representative wells were obtained with an iPhone 4S with an Olloclip Macro lens (10× multiplier).

Chromatin-immunoprecipitation (ChIP) assay. Naive and EM $CD8^+$ T cells (1×10^6 cells per subset) were cultured for 6 h under nonactivating conditions and activating conditions (2 μg/ml anti-CD3 plus 20 μg/ml anti-CD28) in complete RPMI medium (10% AB serum). For inhibition of glucose use, cells were treated with 50 mM 2-DG (Sigma-Aldrich). Cells were then 'snap-frozen' in ethanol-dry ice and stored in minus 80 °C. ChIP assays were done by Active Motif. Cells were fixed with 1% formaldehyde. Chromatin was isolated by disruption of cells with a Dounce homogenizer. Lysates were sonicated and the DNA sheared to an average length of 300–500 bp. Genomic DNA was prepared by treatment of aliquots of chromatin with RNase and proteinase K followed by ethanol precipitation. For ChIP precipitation, chromatin was precleared with protein A agarose beads (Invitrogen) and genomic DNA regions of interest isolated with polyclonal antibody to acetylated H3K9 (53114; Active Motif) or polyclonal antibody to histone H3 (ab1791; Abcam). Complexes were washed, eluted from the beads with SDS buffer and treated with RNAse and proteinase K. The post-ChIP DNA was purified by phenol-chloroform extraction and ethanol precipitation. Quantitative PCR was done in triplicate for specific regions of the *IFNG* promoter with SYBR Green Supermix (Bio-Rad). The following primers were used: IFNG-7 (forward, 5′-TCATCCCTGCCTATCTGTCA-3′, and reverse, 5′-TCCTCTGGCTGCTGGTATTT-3′), IFNG-382 (forward, 5′-CGCATTCTTTCCTTGCTTTC-3′, and reverse, 5′-GGGCCTCTCAAACCTTTACA-3′), IFNG-4179 (forward, 5′-TGGAAGAAATCTACGCCAAAGT-3′, and reverse, 5′-GCAGTCACATCCTAGCACTCA-3′). The resulting signals were normalized for primer efficiency by quantitative PCR for each primer pair with input DNA.

Statistical analysis. Normality of log-transformed data (for IFN-γ secretion) was assessed with the Shapiro-Wilk test; distribution not tested otherwise. Data were assessed with paired two-sided Student's *t*-tests, except for morphometric analyses (for which the Mann-Whitney *U*-test was used). For comparison of increases (before versus after) in paired samples, a simple linear-regression model was used. *P* values of less than 0.05 were considered statistically significant.

50. Bihl, F.K. *et al.* Simultaneous assessment of cytotoxic T lymphocyte responses against multiple viral infections by combined usage of optimal epitope matrices, anti-CD3 mAb T-cell expansion and "RecycleSpot". *J. Transl. Med.* **3**, 20 (2005).

doi:10.1038/ni.2687